Exchange bias anisotropy versus antiferromagnet thickness in uniaxial Cr/Fe bilayers

L. Anghinolfi,[1] F. Bisio,[2,*] M. Canepa,[3] and L. Mattera[3]
[1]*Dipartimento di Fisica, Università di Genova, via Dodecaneso 33, I-16146 Genova, Italy*
[2]*CNR-SPIN, Corso Perrone 24, I-16152 Genova, Italy*
[3]*CNISM, Sede Consorziata di Genova and Dipartimento di Fisica, Università di Genova, via Dodecaneso 33, I-16146 Genova, Italy*
(Received 12 January 2010; revised manuscript received 4 June 2010; published 22 June 2010)

We have investigated the thickness dependence of exchange bias (EB) in ultrathin epitaxial Cr/Fe/Ag(001) bilayers. The system features an artificially patterned structure consisting of coherently aligned nanometric ripples at the Cr/Fe buried interface. The patterning provides an abundance of preferentially aligned steps resulting in both morphological and magnetic uniaxial anisotropies. Increasing the Cr thickness the EB evolves from an uniaxially anisotropic state, in which its magnitude is a function of the field-cooling direction, to an isotropic behavior. We account for this phenomenon invoking a thickness-dependent variation in the spin structure of the antiferromagnet driven by the topological frustration at the stepped Cr/Fe interface.

DOI: 10.1103/PhysRevB.81.224427 PACS number(s): 75.75.−c, 75.60.Jk, 75.30.Et

I. INTRODUCTION

Exchange bias (EB) is one of the most interesting phenomena induced by the exchange coupling at the interface between a ferromagnet (FM) and an antiferromagnet (AF). Discovered more than 50 years ago,[1] EB has been receiving a steady attention ever since due to its scientific relevance and its widespread technological application in the magnetic data storage field.[2–4]

Though a comprehensive model of the phenomenon has not yet been developed, several aspects of EB start to be understood. Many relevant issues remain however open, among which the assessment of the spin structure of the AF counterpart throughout its whole volume,[5–7] and its role in EB.[8–14] Many experiments suggest a strong role of the "bulk" AF spin structure in governing EB,[13,14] opposite to a more intuitive "purely interface" AF effect.[15] Several theoretical models also invoke various spin structure within the AF layer to account for the presence and magnitude of EB.[9–11] Experimentally, however, the direct observation of the AF spin structure is not straightforward, hence the evidence on the role of the AF layer is often indirectly deduced via its influence on the magnetic properties of the FM counterpart.

In this paper we report the AF-thickness dependence of the EB properties of a nanopatterned Cr/Fe/Ag(001) bilayer and propose a model based on a thickness variation in the AF spin structure to account for the observations. In our sample, the buried interface between the Cr and Fe layers is characterized by a nanopatterned structure made of coherently aligned ripples fabricated by the ion sculpting technique.[16] The presence of the interface ripples provides an abundance of aligned monatomic steps, resulting in both morphological and magnetic uniaxial anisotropies,[17] and topological spin frustration at the contact between the two materials.[18,19] As a function of increasing Cr thickness, we observe an evolution of the EB properties. At low Cr coverage, e.g., 2 nm, the EB magnitude and the magnetization reversal mechanisms of the system are strongly dependent on the orientation of the field-cooling (FC) field with respect to the nanoripples, whereas a crossover to isotropic behavior is observed for larger thickness. We propose that this crossover arises from a thickness-dependent variation in the spin structure of the AF layer, driven by the influence of spin frustration at the interface.

II. EXPERIMENT

A. Sample preparation

All the experiments have been performed in an ultrahigh vacuum (UHV) chamber with a base pressure of 1×10^{-10} mbars, described in previous publications.[20,21] The experimental setup allows performing *in situ* magneto-optical Kerr effect (MOKE) with a resolution in external magnetic field **H** of ±0.4 Oe, and features a variable-temperature sample holder goniometer with a $\pm1°$ azimuthal-angle resolution. The Cr/Fe/Ag(001) bilayers described in this work were prepared and measured *in situ* according to the experimental procedures described in detail in Refs. 17 and 20. Here we only recall the main aspects of the sample preparation, referring the reader to our previous work for deeper discussion. First, a 3-nm-thick Fe film was deposited by molecular-beam epitaxy onto a single-crystal Ag(001) surface.[17] Both Fe and Cr grow epitaxially on Ag(001) thanks to the small lattice mismatch.[22,23] After the deposition, the film was irradiated at 350 K with a defocused 1 KeV Ar^+ beam, incident at 70° from the surface normal and along the $[100]_{Fe}$ crystallographic axis. Under these conditions, nanometric ripples oriented along the $[100]_{Fe}$ direction formed at the film surface, with a mean wavelength $\Lambda\approx9$ nm and side walls consisting of crystalline facets at a mean angle $\approx14°$ with respect to the surface normal,[17] as sketched in the topmost left panel of Fig. 1.

Cr films of variable thickness were subsequently deposited on the rippled Fe surface. Initially, a 2-nm-thick Cr film was deposited on the rippled Fe surface at 180 K in order to strongly reduce intermixing effects. The sample was then exposed, at $T=180$ K, to 20 L (1 $L=1\times10^{-6}$ mbar s) of research grade O_2 and subsequently annealed to 670 K. The Auger-electron spectroscopy (AES) spectrum of the surface after this procedure is shown in Fig. 1 (top curve in the right-hand graph). Cr and oxygen AES lines are clearly vis-

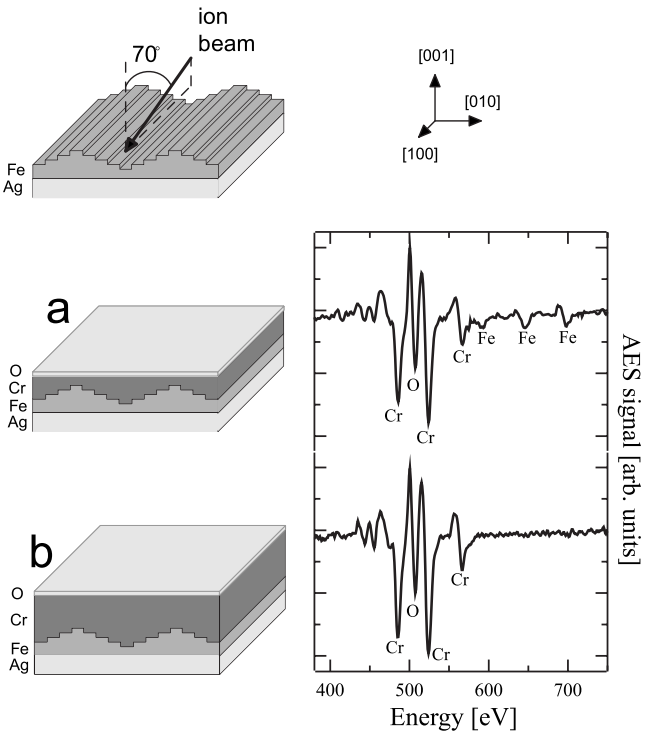

FIG. 1. Left: representative scheme of the morphology of the nanopatterned Cr/Fe/Ag(001) bilayers at various stages of their preparation procedure. Right: AES spectra of the O/(2 nm Cr)/Fe/Ag(001) (top) and of the O/(4.5 nm Cr)/Fe/Ag(001) sample (bottom).

ible, with the residual contribution from the underlying Fe film still present on the high-energy side. Interestingly, upon performing a further deposition of Cr on top of this film at $T=420$ K in absence of any further exposure to O_2, we observe that the intensity of the oxygen Auger line remains unchanged. In the bottom part of the graph we show as an example the spectrum measured for the oxidized Cr/Fe bilayer after the further deposition of 2.5 nm of Cr at $T=420$ K. It can be clearly seen that the intensity of the oxygen AES line has remained identical in the two cases while the Fe contribution has completely vanished. This indicates that oxygen remains segregated at the sample surface during deposition, acting as surfactant for the growth of Cr.[24] The observation of the oxygen surfactant effect suggests that the thickness of the oxidized Cr layer is limited to the surface or the topmost subsurface layer at most.[25] By means of the oxygen-aided growth is therefore possible, once a "seed" Cr layer has been grown, to increase *ad libitum* the thickness of the AF layer while keeping parameters such as buried-interface morphology and surface composition unchanged, as schematically shown by the drawings labeled as "a" and "b" in the left part of Fig. 1. Furthermore, the controlled surface oxidation while having no substantial influence on the underlying Fe layer, prevents any sample surface deterioration over the time required for the measurements (few days under UHV).

Inspection of the low-energy electron-diffraction (LEED) pattern of the O/Cr/Fe system for both Cr thicknesses shows slightly blurred $p(1\times1)$ spots and the absence of whatever superstructure spots, suggesting that the outermost surface is relatively well ordered and devoid of any large-scale morphological feature (like ripples due to conformal Cr growth or agglomerates induced by the annealing).

B. Magnetic properties

Previous studies have shown that nanopatterned Fe/Ag(001) films are endowed with an in-plane magnetic anisotropy energy (MAE) consisting of superimposed biaxial and uniaxial anisotropy contributions.[26,27] The deposition of a Cr overlayer preserves the MAE, only slightly modifying the magnitude of the various contributions.[20] This anisotropy affects the magnetization reversal mechanisms of the system as a function of the relative angle between the external field **H** and the anisotropy axes of the sample. The magnetization reversal, as will be shown in the next section, can proceed via one-step, two-step, or three-step processes that, respectively, involve the nucleation and propagation of 180° domain walls (DWs), 90° DWs, or both.[28]

In this work, in order to avoid any morphology reproducibility issue, we will focus our attention on the EB properties of a *single*, representative nanopatterned Cr/Fe sample prepared according to the above procedure, analyzing the cases of 2 nm and 4.5 nm Cr overlayer thickness, respectively. We will refer to these cases as the 2 and 4 nm case. The EB was induced by subjecting the sample to FC procedures with **H** in the film plane and oriented either along the surface ripples or perpendicular to them (henceforth referred to as $FC_{\parallel}$ and $FC_{\perp}$, respectively). The FC was performed by applying a field of 140 Oe, sufficient for saturating the sample magnetization along the field direction and cooling the sample from 670 to 180 K.

III. RESULTS

A. Thick-antiferromagnet case

We will begin addressing the loops recorded for the 4 nm case, whose features are more straightforward to discuss, and later move to the more involved 2 nm case. In Fig. 2 we report a series of representative hysteresis loops for the Cr/Fe system as a function of the relative angle α between **H** and the $[100]_{Fe}$ high-symmetry direction (nominally coinciding with the ripple orientation) under $FC_{\parallel}$ conditions. The experimental data are reported as the black lines and markers in the left panels while the insets on the right side provide a schematic representation of the measurement geometry and of the FC orientation (the gray stripes indicate the ripple direction). The loops have been measured *in situ* at $T=180$ K with *s*-polarized input radiation. All the loops have been measured by means of sweeping **H** between +140 and −140 Oe; the horizontal scale of the various graphs is adjusted from case to case for better highlighting the loop features. The MOKE signal, to first-order approximation, is proportional to the projection of **M** onto the direction of **H**. All loops have been normalized at saturation. Where applicable, small arrows on the graphs provide a pictorial representation of the orientation of **M** at various stages of the loops.

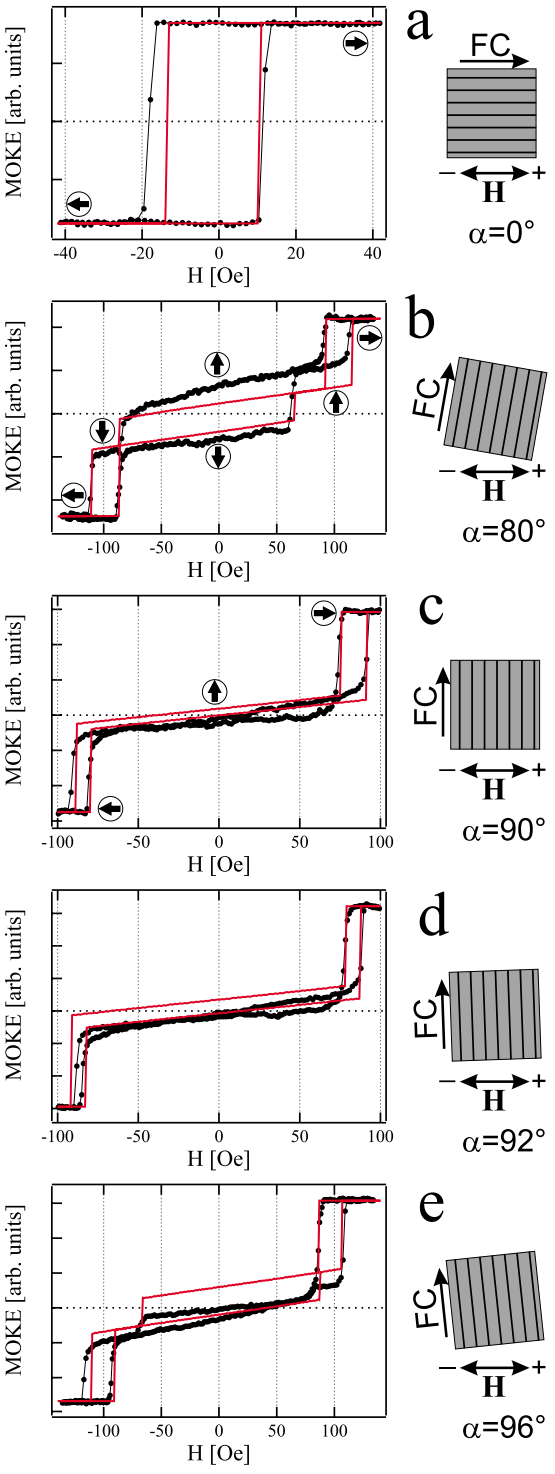

FIG. 2. (Color online) Longitudinal MOKE hysteresis loops measured as a function of the relative angle α between the ripple direction and the applied field **H** for the 4 nm case in the $FC_{\parallel}$ case (black lines and markers). The red (gray) lines are hysteresis loops simulated according to the model described in Sec. III C. The horizontal scale differs from graph to graph.

In loop a, measured for **H** parallel to the ripples, we observe a square loop characterized by a single magnetization jump that corresponds to a one-step reversal process from **M** aligned along antiparallel to parallel orientation to **H**.[28] Loop b, recorded for **H** making an angle $\alpha=80°$ with the ripples, exhibits three magnetization jumps per branch. Starting from the positive saturation, where **M** is roughly perpendicular to the ripples, the first jump corresponds to the alignment of **M** parallel to the ripples, the second to a further a 180° rotation of **M**, and the third to **M** again perpendicular to the ripples.[28] Loops "c" and "d," measured for **H** roughly oriented perpendicular to the ripples, both exhibit a two-step reversal, corresponding to the switching of **M** from perpendicular to parallel to the ripples and from parallel to perpendicular again.[28] Loop "e," finally, is analogous to loop b though some of the transitions are barely discernible in the magneto-optical signal. For all the loops, in between the various irreversible jumps, the smoother variations in the MOKE signal are indicative of coherent **M** rotation.[27] For the sake of clarity, in the following of this paper we will refer to the various irreversible transitions of **M** according to their relative position in the graphs (lateral, central, left, and right).

The asymmetries in the *magnitude* of the MOKE signal in the loops are due to second-order magneto-optical effects[29] quite common in anisotropic systems and not to EB. The presence of EB in these loops, instead, is manifest through the appearance of various kinds of asymmetries in the **H** values corresponding to irreversible **M** transitions, as expected for biased systems with complex anisotropy like ours.[30] In loop a, EB shifts the loop by 3.5 Oe toward the negative **H** values. For loop b, the situation gets much more involved. Here the two "lateral" transitions do not occur at the same absolute value of field but appear collectively shifted by a small amount toward the positive **H** direction while the central transition is significantly shifted to negative **H** values. In loop c, no significant shifts of the lateral transitions occur but the "right" coercive field is significantly larger than the "left" coercive field. In loop d, measured at an angle α differing by merely 2° with respect to loop c, the same situation occurs but the values of coercive field are smaller by a factor 2 with respect to the previous case. Finally, in loop e the two lateral transitions appear collectively shifted toward negative **H** values while no clear statements can be made for the central ones.

In Fig. 3, we report a set of hysteresis loops measured under the same conditions as above but having changed the FC orientation to $FC_{\perp}$. Also in this case, the reversal of **M** can occur via one-step, two-step, or three-step processes, in perfect analogy to the previous case. The effects of the different FC direction with respect to Fig. 2, however, consistently modify the asymmetries observed in the loops.

Loop a is again square and slightly shifted toward negative field values, though less than its counterpart of Fig. 2 ($\approx$1 Oe). In loop b, the "lateral" transitions are shifted toward negative **H** while the central ones appear well centered. In loop c, the left and right coercive fields are this time almost equal, but the transitions are collectively shifted toward negative field, and the same substantially occurs for loop d, though with significantly smaller coercive fields. Finally, in loop e, the two lateral transitions again appear collectively shifted toward negative field and exhibit a similar coercive field while no definite statement can be made for the central ones. In both cases of Figs. 2 and 3, the magnetization "jumps" are fairly sharp and well defined.

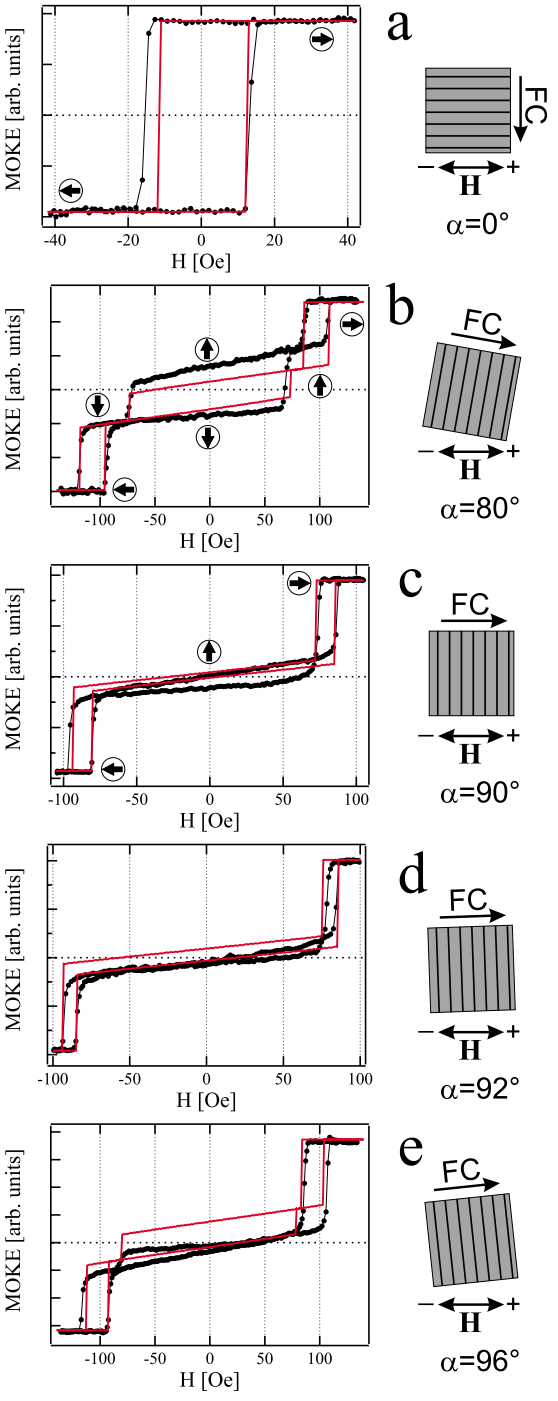

FIG. 3. (Color online) Longitudinal MOKE hysteresis loops measured as a function of the relative angle α between the ripple direction and the applied field **H** for the 4 nm case in the $FC_{\perp}$ case (black lines). The red (gray) lines are hysteresis loops simulated according to the model described in Sec. III C. The horizontal scale differs from graph to graph.

B. Thin-antiferromagnet case

In Fig. 4 we report sets of longitudinal MOKE hysteresis loops measured in the 2 nm situation as a function of the azimuth angle α, under experimental conditions identical to the ones specified for the 4 nm case. The loops reported as full black symbols in Fig. 4 have been measured under $FC_{\perp}$ conditions while the open blue (dark gray) symbols correspond to loops recorded for $FC_{\parallel}$ (arrows of corresponding color in the right-hand diagrams point in the respective FC direction). At a first glance, some of the loops appear different with respect to the 4 nm case and, more interestingly, marked differences also appear when comparing the $FC_{\perp}$ and $FC_{\parallel}$ cases.

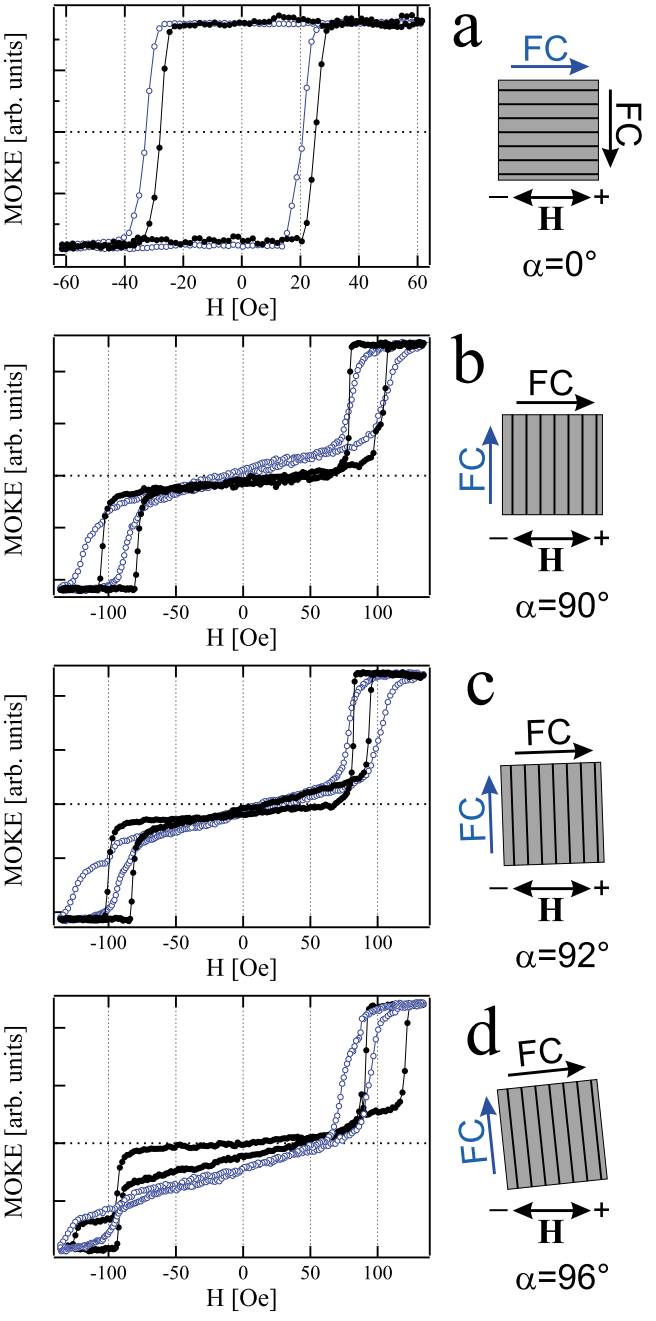

FIG. 4. (Color online) MOKE hysteresis loops measured, in the 2 nm case, as a function of the relative angle α between the ripple direction and **H**, under $FC_{\perp}$ (full black symbols) and $FC_{\parallel}$ [open blue (dark gray) symbols] conditions.

In the $FC_{\perp}$ case, the general trend of loop shape vs α appears preserved with respect to the 4 nm case, and the transitions between the various orientations of **M** are still quite sharp. However, at variance with before, the asymme-

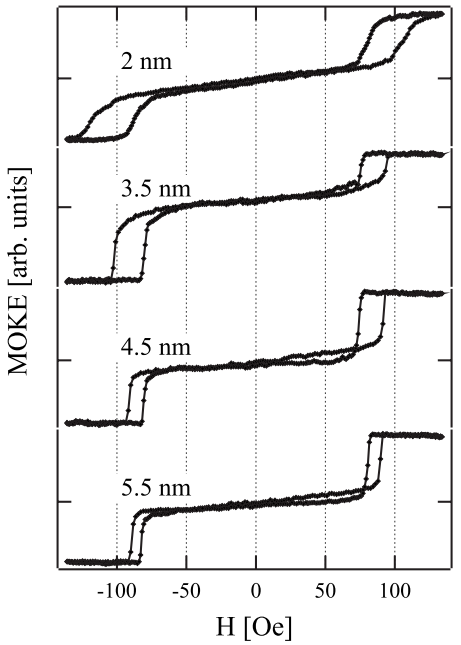

FIG. 5. MOKE hysteresis loops as a function of Cr thickness. The loops have been measured at $T=180$ K for $\alpha=90°$ following a $FC_{\|}$ procedure. The AF thickness is indicated for each loop on the graph.

tries in the transition fields are either absent within our experimental accuracy (loops b and d) or at best barely discernible (loops a and c). The large asymmetry of the MOKE magnitude in loop d is due to magneto-optical effects rather than EB. This suggests a strong reduction in the EB-induced unidirectional anisotropy contribution with respect to the 4 nm case.

The situation changes drastically for the case of FC parallel to the ripple ridges [open blue (dark gray) markers]. Here, loop a is still square, with relatively sharp transitions and is shifted toward the negative field direction by ≈6 Oe. The other loops, while still retaining the characteristic split shape arising from the system's anisotropy, exhibit severely broadened magnetization jumps. Under these conditions, it is difficult to quantify the presence of EB asymmetries in the loops, though they clearly appear in loops c and d, where the lateral transitions are collectively shifted toward negative fields. The broadening of the transitions and any asymmetry in the critical field for magnetization reversal disappear upon heating the sample above the blocking temperature [$T \approx 300$ K (Ref. 20)], where sharp magnetization jumps in the loops are restored.

In terms of Cr thickness, the broadening of the transitions, so apparent in the 2 nm case, quickly fades with increasing thickness. In Fig. 5 we report a set of hysteresis loops measured for $\alpha=90°$ after a FC parallel to the ripples as a function of various AF-thickness values on the same Cr/Fe sample. In the 2 nm case just discussed, the broadening of the transitions is very pronounced. This effect has already almost completely disappeared for 3.5 nm Cr, and the **M** transitions stay sharp upon a further increase in thickness (4.5 and 5.5 nm Cr) upon which only a gradual decrease in coercive field is observed.

C. Model

In order to rationalize the mechanisms of EB in this system, we have applied a simple model of magnetization reversal already successfully applied to thin-film systems.[27,28]

This model assumes the system to be in a single-domain state of uniform, saturated magnetization, that can be characterized by indicating the direction of **M** in the film plane. The free-energy density f of the system is then written as the sum of the anisotropy K and the Zeeman contributions as

$$f = K(\phi) - \mathbf{H} \cdot \mathbf{M}, \tag{1}$$

where ϕ is the angle between the magnetization **M** and the $[100]_{Fe}$ direction. As the external field is swept, **M** is allowed to change orientation following a *local* minimum of f. In addition, for every value of **H**, **M** is allowed to jump to a more favorable energy minimum, provided it exists, by the displacement of a domain wall. This process requires a finite activation energy E_{DW} so it can occur only when the energy difference between the two minima reaches a certain critical value. E_{DW}, and accordingly the coercive fields, is unrelated to the magnetic anisotropy and not known *a priori* but it can be deduced from the experimental values of the switching fields in the hysteresis loops. The physically relevant quantities, as long as this work is concerned, are the activation energy for a 90° DW E_{DW}^{90} and for a 180° DW E_{DW}^{180}.

The magnetic anisotropy energy of the films can be written as[17,20,27]

$$K(\phi) = \frac{K_c}{4}\sin^2 2\phi + K_u \sin^2 \phi + K_k \sin^2\left(\phi + \frac{\pi}{4}\right) + \\ - \frac{J}{t_{FM}}\cos(\phi - \phi_{eb}), \tag{2}$$

where K_c is the biaxial anisotropy constant, with easy axis along the $[100]_{Fe}$ (and equivalent) directions, K_u is the ripple-induced uniaxial anisotropy, with easy axis along the ripple ridges,[17] K_k is the anisotropy associated with atomic kink sites along the ripple edges,[27] and the last term is the unidirectional anisotropy due to EB, where ϕ_{eb} is the angle that **H** forms with the $[100]_{Fe}$ direction during the FC, t_{FM} is the FM thickness and J is the strength of the EB coupling.[20]

We performed a best-fit procedure for the 4 nm case (the loops reported in Figs. 2 and 3) optimizing the anisotropy constants and J in Eq. (2). The best-fit simulated loops are reported as red (gray) lines in Figs. 2 and 3, corresponding to the anisotropy values and activation energies reported in Table I. The EB unidirectional anisotropy pointed along the $[100]_{Fe}$ direction in the $FC_{\|}$ and along the $[010]_{Fe}$ direction in the $FC_{\perp}$ case but with identical magnitude, in agreement with Ref. 20. A comparison between experimental and simulated coercivity H_C and EB values for a broader α range with respect to the one of Figs. 2 and 3 is reported in Fig. 6, limited for the sake of clarity to the lateral transitions only. The $80°-100°$ α interval, though limited, provides abundant information on the system's anisotropy. In fact both double-jump and triple-jump **M** reversals occur within this range, and the α value at which the crossover between the two regimes is found is extremely sensitive to the overall

TABLE I. Best-fit values for the anisotropy constants in Eq. (2).

K_c (10^5 erg/cm^3)	K_u (10^5 erg/cm^3)	K_k (10^5 erg/cm^3)	J (10^{-3} erg/cm^2)	$\frac{E_{DW}^{90}}{M_S}$ (Oe)	$\frac{E_{DW}^{180}}{M_S}$ (Oe)
3.9	1.35	0.3	1.7	9.0	24.0

anisotropy.[28] Whereas it might be desirable to extend the measurement to the whole α range,[30] in our case for α outside the $80°-100°$ interval the lateral transitions occur at increasingly larger **H** values exceeding ± 140 Oe, for which our setup does not allow their measurement with the resolution needed to resolve the small EB.

The anisotropy values agree well with previous results,[17,20,27] and we will not discuss them further (the finite kink anisotropy constant can be ascribed to a misalignment on the order of $1°-2°$ between the macroscopic ripple orientation and the $[100]_{Fe}$ direction).

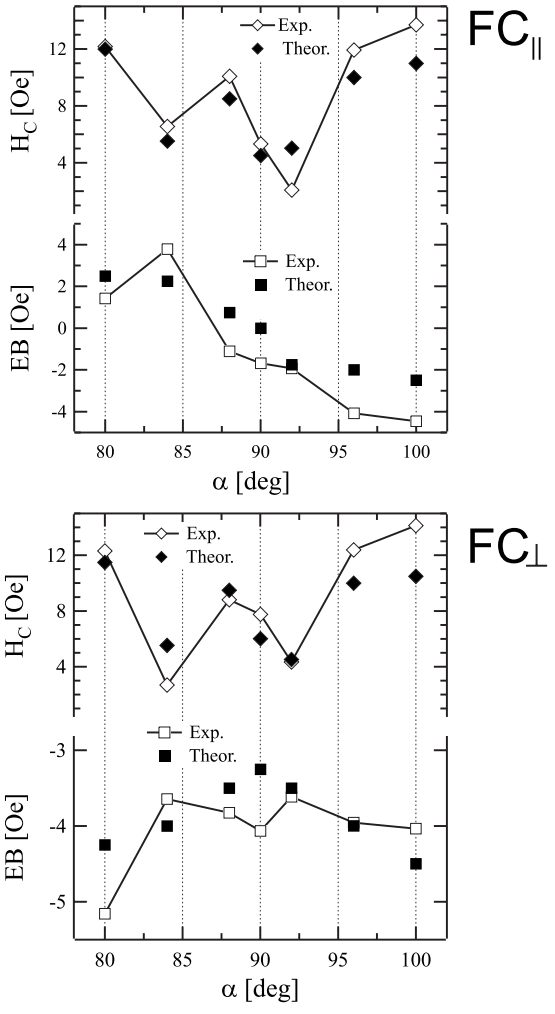

FIG. 6. Top panel: experimental (open symbols) and simulated (full symbols) values of coercivity (diamonds) and exchange bias (squares) for the lateral transitions as a function of the angle α, in the 4 nm $FC_{\parallel}$ case. Bottom panel: experimental (open symbols) and simulated (full symbols) values of coercivity (diamonds) and exchange bias (squares) for the lateral transitions as a function of the angle α, in the 4 nm $FC_{\perp}$ case.

We observe that the model reproduces well the complex pattern of asymmetries of the central and lateral transitions and, where applicable, the asymmetries between left and right coercive fields, a remarkable achievement considering that Eq. (2) represents a first-order MAE approximation and that both the $FC_{\parallel}$ and the $FC_{\perp}$ data were reproduced using a single set of parameters. The explicit inclusion of DW activation energies allows to obtain meaningful anisotropy constants, avoiding the underestimations typical of coherent models, and also decouples the coercivity and anisotropy of the system. Interestingly, we notice that the largest discrepancies between experiment and model are observed in the case of the perfectly square loops ($\alpha=0$), i.e., in the simplest case (they are, however, visually enhanced by the restricted **H** range of the graph). This apparent shortcoming can be explained keeping in mind that the fit parameter that determines the coercive field in the $\alpha=0$ case, i.e., the E_{DW}^{180} energy, is also responsible for determining the location in **H** of the central transitions in other hysteresis loops. The best-fit parameters minimize the errors over the whole data set and not only for $\alpha=0$, hence the "discrepancy" for some of the loops. We can, however, safely infer from the comparison of experiment and simulation that, in the 4 nm case, performing FC procedures either parallel or orthogonal to the ripple direction does not lead to different magnitude of EB, nor to any difference in the magnetization reversal mechanism, that occurs in both cases by unrestrained propagation of DWs at well-defined critical-field values. Hence the EB can be in this case labeled as "isotropic."

Shifting to the 2 nm case, we immediately notice that reproducing the hysteresis loops in both the $FC_{\parallel}$ and $FC_{\perp}$ cases with a single set of parameters is an impossible achievement. This for two specific reasons: first, there is an apparent difference in the EB coupling in the two cases, as evidenced by the very different degree of asymmetries observed in the two loop sets. Second, it is apparent from the loops that for the $FC_{\parallel}$ case the DW processes substantially differ with respect to all the other cases shown. No sharp transitions indicative of free DW propagation after unpinning are observed but it rather seems that several pinning centers are present that hinder the unrestrained DW propagation. This is a situation that does not even match the physical assumptions of our simple model, especially since this behavior is apparently not intrinsic to the system but depends on the type of FC performed. It is therefore clear that "anisotropic" EB appears in the 2 nm case as a function of the FC direction (this "EB anisotropy" is not to be confused with the magnetic anisotropy, which is an intrinsic system's property not dependent on EB).

IV. DISCUSSION

We begin the discussion recalling that the 4 and 2 nm data reported here were measured on the same sample. This im-

plies that morphological parameters such as Fe thickness, ripple structure, and any characteristics of the buried Cr/Fe interface (sharpness, density, type of defects, etc.) are identical in the two cases. We also recall that AES and LEED data suggest that in both cases the Cr overlayer was continuous and exhibited an outer surface devoid of morphological features. Thus, the thickness-dependent variations in the EB properties are most likely a consequence of a thickness-dependent variation in the AF spin structure.

In our experiment, the interface between the two materials is characterized by a great abundance of terraces separated by coherently aligned monatomic steps. Upon contact with Cr that in the bulk features the well-known layered-AF structure within {001} planes,[31–33] a significant spin frustration is expected. Given the large DW thickness in Cr,[34] such a frustration will not relax via the formation of step-induced DWs (Refs. 18 and 35) but rather via some complex rearrangement of the spins in proximity of the stepped interface.[19] For very thin Cr layers onto stepped Fe,[19] such a spin reorientation can be so severe to make the layered-AF structure of Cr barely recognizable. As the Cr thickness is increased, though the topological frustration persists, the minimization of the exchange energy throughout the whole AF layer should gradually lead to a spin structure more alike the bulk one, even in proximity of the buried interface.

In this model, the AF spin structure in the 2 nm case is therefore still strongly influenced by the magnetic state at the Cr/Fe interface, possibly yielding different interface spin configurations for FM magnetization aligned either parallel or perpendicular to the steps. We therefore suggest that following a $FC_{\parallel}$ or a $FC_{\perp}$ procedure, respectively, the spin structures that are "frozen" within the Cr/Fe junction are different. Such a difference can justify the different density of pinned uncompensated spins, accordingly accounting for the different magnitude of the EB coupling in the two cases.

In the 4 nm case, the EB magnitude is instead independent of the FC direction, within our accuracy, a phenomenon already reported in Ref. 20. This means that there is a thickness-dependent crossover from the anisotropic to isotropic EB behavior. We tentatively ascribe such crossover to the achievement by the AF layer of a "bulklike" layered-AF spin structure with increasing thickness. In this situation the topological frustration due to the stepped interface persists but the AF spin structure exhibits a weaker sensitivity with respect to the underlying orientation of the FM magnetization. To the first order, in fact, identical excess exchange energy is expected for **M** parallel or perpendicular to the ripple ridges for bulklike arrangements of Cr and Fe spins. This weak dependence is then reflected in the isotropic EB behavior.

A further issue of interest is the different sharpness of the magnetization reversal jumps observed in the data. In systems for which magnetization reversal occurs via DW processes, like ours, the presence of sharp or blurred **M** jumps is a function of the density and type of defects (typically morphological or structural) in the material, that act as DW-pinning centers.[36] Morphological/structural defects are surely present within the Cr/Fe junction but their density does not depend on factors like the FC direction. Considering the 2 nm case, this suggests that the different sharpness of the **M** jumps for $FC_{\parallel}$ or $FC_{\perp}$ is related to the formation of DW-pinning centers of magnetic origin, whose type and/or density is related to the spin structure of the system. Thus, a correlation between the magnitude of the EB for $FC_{\parallel}$ and $FC_{\perp}$ and the blurring of the **M** transitions is apparent, where the frozen uncompensated AF spins responsible for the EB act as effective DW-pinning centers, a hypothesis supported by the recovery of sharp transitions above the blocking temperature. In this picture, larger EB would therefore imply higher density of pinning centers that hinder the free DW propagation causing a more pronounced broadening of the magnetization jumps and *vice versa*. Such a pinning might be effective for DWs propagating either across the FM or the AF layers: though MOKE probes only the FM behavior, DWs in the two layers can be in fact effectively coupled by an exchange-spring mechanism.[37] In this respect, the recovery of the isotropic behavior in the jump sharpness observed for the thick-AF case could either be due to the weakening of the exchange-spring coupling or the decreased sensitivity of AF DWs to the pinned spins at the interface that occur upon the achievement of a bulklike AF spin structure.

One final issue to address concerns the crossover thickness from the partly disordered to the bulklike AF behavior. According to the loops reported in Fig. 5, the transition to a bulklike AF spin structure is already attained for Cr a thickness of 3.5 nm, thereby locating such a crossover thickness in the range between 2 and 3.5 nm. The thickness range below 2 nm Cr, that would be very interesting to investigate for determining the critical thickness for the onset of the EB,[2] could not be successfully addressed in this study due to the onset of morphological instabilities in the system upon annealing (formation of agglomerates, interdiffusion) that precluded a safe evaluation of the data.

V. CONCLUSIONS

In summary, we have measured the magnetic properties of epitaxial Cr/Fe/Ag(001) exchange-biased systems featuring a uniaxially nanopatterned Cr/Fe interface as a function of varying thickness of the AF overlayer. Employing fully epitaxial system and a surfactant-aided procedure for the Cr growth enabled us to systematically explore the effect of changing the AF layer thickness while keeping the morphology of the whole system under highly controlled conditions. Going from thin (2 nm) to thicker (4.5 nm) Cr films, we observed a crossover between a state in which the EB properties were anisotropic with respect to the FC direction, to a state in which an isotropic behavior was observed.

We accounted for this observation by postulating a thickness dependence of the spin structure of the AF layer. For the smaller coverage, we propose that the AF spin structure is still dominated by the frustration effects at the stepped Cr/Fe interface whereas a more bulklike structure is gradually recovered for thicker layers.

ACKNOWLEDGMENTS

Financial support from the Università di Genova (PRA 2008), the Fondazione Carige and the MIUR program PRIN 2008 no. 2008AKZSXY_002 is acknowledged.

*bisio@fisica.unige.it

[1] W. H. Meiklejohn and C. P. Bean, Phys. Rev. **102**, 1413 (1956).
[2] J. Nogués and I. K. Schuller, J. Magn. Magn. Mater. **192**, 203 (1999).
[3] V. Skumryev, S. Stoyanov, Y. Zhang, G. Hadjipanayis, D. Givord, and J. Nogués, Nature (London) **423**, 850 (2003).
[4] C. Chappert, A. Fert, and F. N. van Dau, Nature Mater. **6**, 813 (2007).
[5] F. Nolting, A. Scholl, J. Stöhr, J. W. Seo, J. Fompeyrine, H. Siegwart, J. P. Locquet, S. Arders, J. Lüning, E. E. Fullerton, M. F. Toney, M. R. Scheinfein, and H. A. Padmore, Nature (London) **405**, 767 (2000).
[6] C. L. Chien, V. S. Gornakov, V. I. Nikitenko, A. J. Shapiro, and R. D. Shull, Phys. Rev. B **68**, 014418 (2003).
[7] M. R. Fitzsimmons, D. Lederman, M. Cheon, H. Shi, J. Olamit, I. V. Roshchin, and I. K. Schuller, Phys. Rev. B **77**, 224406 (2008).
[8] A. P. Malozemoff, Phys. Rev. B **35**, 3679 (1987).
[9] D. Mauri, H. C. Siegmann, P. S. Bagus, and E. Kay, J. Appl. Phys. **62**, 3047 (1987).
[10] M. D. Stiles and R. D. McMichael, Phys. Rev. B **59**, 3722 (1999).
[11] U. Nowak, K. D. Usadel, J. Keller, P. Miltényi, B. Beschoten, and G. Güntherodt, Phys. Rev. B **66**, 014430 (2002).
[12] M. Ali, C. H. Marrows, M. Al-Jawad, B. J. Hickey, A. Misra, U. Nowak, and K. D. Usadel, Phys. Rev. B **68**, 214420 (2003).
[13] C. W. Leung and M. G. Blamire, Phys. Rev. B **72**, 054429 (2005).
[14] R. Morales, Z.-P. Li, J. Olamit, K. Liu, J. M. Alameda, and I. K. Schuller, Phys. Rev. Lett. **102**, 097201 (2009).
[15] T. C. Schulthess and W. H. Butler, Phys. Rev. Lett. **81**, 4516 (1998).
[16] U. Valbusa, C. Boragno, and F. Buatier de Mongeot, J. Phys.: Condens. Matter **14**, 8153 (2002).
[17] F. Bisio, A. Toma, R. Moroni, R. Pasero, F. Buatier de Mongeot, C. Boragno, M. Canepa, U. Valbusa, and L. Mattera, Phys. Rev. B **75**, 054407 (2007).
[18] A. Vega, D. Stoeffler, H. Dreyssé, and C. Demangeat, Europhys. Lett. **31**, 561 (1995).
[19] R. Robles, E. Martínez, D. Stoeffler, and A. Vega, Phys. Rev. B **68**, 094413 (2003).
[20] F. Bisio, L. Anghinolfi, M. Canepa, and L. Mattera, Phys. Rev. B **79**, 054407 (2009).
[21] F. Bisio, S. Terreni, M. Canepa, and L. Mattera, Phys. Rev. B **72**, 174413 (2005).
[22] M. Canepa, S. Terreni, P. Cantini, A. Campora, and L. Mattera, Phys. Rev. B **56**, 4233 (1997).
[23] R. Pfandzelter, T. Igel, and H. Winter, Surf. Sci. **375**, 13 (1997).
[24] R. Moroni, F. Bisio, M. Canepa, and L. Mattera, Nucl. Instrum. Methods Phys. Res. B **193**, 480 (2002).
[25] H. L. Meyerheim, D. Sander, R. Popescu, W. Pan, I. Popa, and J. Kirschner, Phys. Rev. Lett. **99**, 116101 (2007).
[26] F. Bisio, R. Moroni, F. Buatier de Mongeot, M. Canepa, and L. Mattera, Appl. Phys. Lett. **89**, 052507 (2006).
[27] R. Moroni, F. Bisio, F. Buatier de Mongeot, C. Boragno, and L. Mattera, Phys. Rev. B **76**, 214423 (2007).
[28] R. P. Cowburn, S. J. Gray, and J. A. C. Bland, Phys. Rev. Lett. **79**, 4018 (1997).
[29] R. M. Osgood III, S. D. Bader, B. M. Clemens, R. L. White, and H. Matsuyama, J. Magn. Magn. Mater. **182**, 297 (1998).
[30] T. Mewes, H. Nembach, J. Fassbender, B. Hillebrands, J.-V. Kim, and R. L. Stamps, Phys. Rev. B **67**, 104422 (2003).
[31] E. Fawcett, Rev. Mod. Phys. **60**, 209 (1988).
[32] J. Unguris, R. J. Celotta, and D. T. Pierce, Phys. Rev. Lett. **69**, 1125 (1992).
[33] H. Zabel, J. Phys.: Condens. Matter **11**, 9303 (1999).
[34] R. Ravlić, M. Bode, A. Kubetzka, and R. Wiesendanger, Phys. Rev. B **67**, 174411 (2003).
[35] H. Hopster, Phys. Rev. Lett. **83**, 1227 (1999).
[36] J. Pommier, P. Meyer, G. Pénissard, J. Ferré, P. Bruno, and D. Renard, Phys. Rev. Lett. **65**, 2054 (1990).
[37] V. I. Nikitenko, V. S. Gornakov, A. J. Shapiro, R. D. Shull, K. Liu, S. M. Zhou, and C. L. Chien, Phys. Rev. Lett. **84**, 765 (2000).